A stochastic model of nitrate transport and cycling at basin scale

Gianluca Botter,[1] Tommaso Settin,[1] Marco Marani,[1] and Andrea Rinaldo[1]

Received 18 September 2005; revised 23 January 2006; accepted 25 January 2006; published 25 April 2006.

[1] A stochastic framework for modelling catchment-scale hydrologic and nitrate responses (as a byproduct of transport processes and of a biogeochemical model of nitrogen cycling and transformations in heterogeneous soils) is proposed and applied to a 53 km^2 basin in northeastern Italy, where observational data and complex land-use distribution and geomorphology demand suitable descriptions. The model is based on a geomorphological scheme of the hydrologic response coupled with suitable Lagrangian transport models (mass-response functions) applied in a Montecarlo framework which explicitly addresses the random character of the processes controlling nitrate generation to the hydrologic cycle, and its transformations and transport. This is obtained by coupling the stochastic generation of climatic and rainfall series with the hydrologic and biogeochemical models. Special attention is devoted to the spatial and temporal variability of nitrogen sources of agricultural origin and to the effects of the relative timing and intensity of the forcing rainfall fields on the ensuing nitrate leaching. The influence of random climatic variables on biogeochemical processes affecting the nitrogen cycle in the soil-water system (e.g., plant uptake, nitrification and denitrification, mineralization) is also considered. Besides its conceptual interest, the relevance of the model stems from the capabilities of estimating the return period of nitrate loads to the receiving water body and the probability distribution of the variables computed. We found that the modes of nitrogen injection through fertilization significantly affect the form of probability distribution of nitrate contained in soil moisture even when the total amount is fixed. As a result, the return period of the water volumes discharged and of the nitrate loads released (in this case into the Venice lagoon) can be linked directly to the ongoing climatic and agricultural regimes, with implications for sustainable management practices.

Citation: Botter, G., T. Settin, M. Marani, and A. Rinaldo (2006), A stochastic model of nitrate transport and cycling at basin scale, *Water Resour. Res.*, *42*, W04415, doi:10.1029/2005WR004599.

1. Introduction

[2] The simulation of likely scenarios can greatly enhance the soundness and sustainability of remediation strategies aimed at improved management of water resources. Given the time required, and the costs involved, in large-scale collection of coherent observations, one can hardly overestimate the importance of models in supporting environmental policies. In this paper we address the setting of a significant stochastic framework for the estimation of loads of solute matter (largely of anthropogenic origin) within hydrologic flows of heterogeneous watersheds. These demand both the explicit description of spatially distributed information (on soils, land use, geomorhology, rainfall etc.) and the predictability stemming from lumped descriptions, echoing similar issues in hydrologic modeling [*Rodriguez-Iturbe et al.*, 1988, 1999].

[3] High nitrate concentrations in agricultural soils are eminently due (directly or indirectly) to the (often excessively) large amount of nitrogen introduced into the environment as fertilizer. High concentrations of NO_3^- in soils can alter the chemical balance of ecosystems, with long-lasting consequences for the biota. The soil nitrogen pool, in fact, is involved with several biogeochemical processes through which the ecosystem retains long memory of external disturbances [e.g., *Porporato et al.*, 2003; *Manzoni et al.*, 2004]. Conversely, because the ion NO_3^- is highly soluble under ordinary conditions, nitrates temporary detained within the soil moisture may be also transferred to the circulating water carrier through various physical and/or chemical processes. Enhanced NO_3^- leaching may cause environmental impacts, such as those causing anoxia and eutrophication of receiving water bodies. Theoretical and experimental evidences suggest that nitrates releases from river basins much depend on runoff from flood events, owing to the simultaneous increase of flux concentrations and of water flowrates. Modelling nitrate fate at the catchment scale thus requires an integrated approach able to describe biogeochemical and hydrological processes in the whole soil-water system, that is, including the effects of both generation units like hillslopes and channeled routing units. A number of existing models [e.g., *Pastor and Post*, 1986; *Vanclooster et al.*, 1995] are specifically aimed at describing the nitrogen cycle both in forested and agricultural soils. Only a few, however, allow for the integrated study at the catchment-scale [e.g., *Whitehead et al.*, 1998; *Birkinshaw and Ewen*, 2000a]. They are usually applied to provide deterministic estimates of relevant hydrologic and

[1]Dipartimento di Ingegneria Idraulica, Marittima e Geotecnica and International Centre for Hydrology "Dino Tonini," Università di Padova, Padova, Italy.

0043-1397/06/2005WR004599

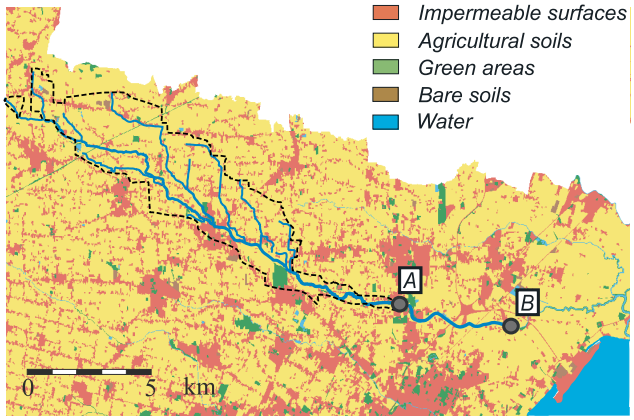

Figure 1. Spatial distribution of soil uses in the Dese catchment (the watershead is labelled by dotted lines). Sections *A* and *B* represent, respectively, the outlet chosen for this application, and the outlet of the hydraulic system (the Dese-Zero river basin) described by *Rinaldo et al.* [2006b]. Note that we have refrained from simulating the system at *B*, where observations are available, to avoid tidal effects (nonexistent at *A* owing to a sizable drop in elevation) which would becloud the main issue of this paper. A proper description of the site location and of the geomorphology involved can be found in *Rinaldo et al.* [2006b].

chemical fluxes on the basis of field observations [e.g., *Birkinshaw and Ewen*, 2000b; *Kurz et al.*, 2005; *Jordan and Smith*, 2005]. Moreover, the influence of the probabilistic character of the undergoing hydrological processes on the nutrient cycle in natural, water-limited ecosystems has been recently investigated [*Rodriguez-Iturbe et al.*, 1999; *Porporato et al.*, 2003; *D'Odorico et al.*, 2003; *Manzoni et al.*, 2004].

[4] In this paper, the impact of random additions of rainfall and fertilizer (thought of as a byproduct of agricultural management) on basin-scale nitrate leaching is investigated in a probabilistic framework by means of a continuous, geomorphologically-based, Montecarlo approach, which explicitly embeds the random character of the climatic and rainfall variables controlling nitrate generation, transformation and leaching. Special attention is devoted to the spatio-temporal variability of the nitrogen sources of agricultural origin (section 2) and to the effect of the temporal distribution of the rainfall fields on the nitrate releases through the hydrologic response (section 3). The influence of random climatic variables on biogeochemical processes occurring in the soil-water system, which are deemed relevant for the ammonia and nitrogen cycling, is also considered. The probabilistic framework adopted here is similar to that employed in a different context by *Rodriguez-Iturbe et al.* [1999], *D'Odorico et al.* [2003], and *Porporato et al.* [2003] for modelling the biogeochemical cycles of the broad-leafed savanna. Differently from *D'Odorico et al.* [2003], however, we model nested subbasins with different geomorphic features and land use - thereby tackling complex settings - and the probabilistic structure of the soil moisture and nitrogen is estimated through a numerical Mont procedure. The Montecarlo forcing is given by rainfall and climate variability summarized by a classic point model [*Rodriguez-Iturbe et al.*, 1987, 1988]. Moreover, we neglect the influence of carbon cycling on nitrate leaching. The latter seems like a reasonable assumption in agricultural catchments where the nutrient cycle is strongly dominated by recurrent anthropogenic disturbances.

[5] The test catchment employed is the Dese river basin closed at Villa Volpi (section *A* in Figure 1), a 53 km^2 wide catchment which is part of a hydraulically complex mainland system discharging into the Venice Lagoon, the Dese-Zero river basin (whose closure is represented by section B in Figure 1). Note that the spatial distribution of the different soil coverages is derived via suitable remote sensing. The presence of extensive agricultural activities produces chronically high concentrations of nitrates in the water flow; as a consequence, eutrophication phenomena have been progressively increasing during the last decades in the receiving water body, the Venice Lagoon, and in the drainage network of its contributing mainland. Given the fragile characters of tidal environments, the development of management practices aimed at controlling water pollution in the Venice Lagoon is deemed an objective of widely acknowledged importance. The reader is referred to *Botter et al.* [2005] and *Rinaldo et al.* [2005, 2006a, 2006b] for further details about the catchment, the remote sensing employed, the observational evidence (gathered at the tidal section B in Figure 1) and the reliability of the modeling tools for single, gauged events.

2. Nitrate Cycling in Catchments

[6] External inputs of nitrogen, *N*, in unmanned vegetated soils derive from precipitation, atmospheric deposition of N_2 and biological fixation of gaseous nitrogen. Because in many circumstances nitrogen is the limiting factor for the primary productivity of the ecosystem, in agricultural soils the crops nitrogen demand is supplied by organic and/or mineral fertilizations. The resulting external *N* loads of anthropogenic origin are usually much larger than other atmospheric inputs and produce remarkably high nitrogen concentrations in the soil-water system. External nitrogen inputs into the ecosystem are transformed by complex internal processes which control both the availability for the biota and the intensity of the *N* losses from the soil. The internal cycling of nitrogen in the soil-water system is characterized by a variety of biological and chemical processes, through which organic nitrogen is oxydated to inorganic *N* (i.e., ammonia and nitrates) available to plant uptake. Conversely, other biological processes lead to the $N - NO_3$ transformation into ammonia ($N - NH_4$) and to the subsequent reduction of the ammonia to organic nitrogen immobilized by the biomass. Nitrogen losses at catchment scales, instead, are chiefly due to nitrate leaching through runoff and, only to a lesser extent, to ammonia volatilization and denitrification processes occurring within saturated zones due to anaerobic processes.

[7] Our aim is to provide catchment-scale estimates of nitrogen cycling. On the basis of the underlying network structure, the test catchment (section 4) is partitioned into 17 subbasins (i.e., source areas) whose average size is of a few km^2 at most, owing to hydrologic constraints - the size of the source area is smaller than the correlation scale of

Table 1. Average N Loads and Fertilization Periods for the Different Crops Identified in the Dese Catchment[a]

Crop	N Load, kg ha^{-1} year^{-1}	Fertilization Period	Relative Extension
Maize	200–300	Spring	34%
Wheat	100–150	Spring and Autumn	11%
Sugar beat	100–150	Spring	19%
Soybean	0	Autumn	10%

[a]The last column indicates the relative extension of each crop in the test catchment.

intense rainfall events [*Rinaldo et al.*, 2006b]. Source areas are characterized by heterogeneous soil types and uses which have been carefully detected by the use of remotely sensed data. Each subbasin is modelled as an individual control volume, where a mass balance is carried out. Each control volume corresponds to the hydrologically and biologically active top soil layer in the considered subbasin, whose estimated thickness, Z_r, is about 30 cm [*Rinaldo et al.*, 2006b]. The nitrogen budget in the soil-water system is chiefly due to nitrates ($N - NO_3^-$) dissolved in the soil moisture and ammonia ($N - NH_4^+$) sorbed on the mineral components of soil. The temporal evolution of the nitrate and ammonia concentrations within each subbasin is provided by:

$$\frac{d[NO_3]}{dt} = F_{[NO_3]} - DENIT - PU_{[NO_3]} + NIT - \frac{Q_{[NO_3]}}{Z_r} \quad (1)$$

$$\frac{d[NH_4]}{dt} = F_{[NH_4]} + MIN - PU_{[NH_4]} - NIT - VOLA \quad (2)$$

where $[NO_3^-]$ and $[NH_4^+]$ are the nitrate and ammonia concentrations in the soil-water system (expressed in mass per unit soil volume $[M][L^{-3}]$), $F_{[NO_3]}$ and $F_{[NH_4]}$ are the nitrate and the ammonia inputs introduced as fertilizers, $PU_{[NO_3]}$ and $PU_{[NH_4]}$ are the rates of nitrate and ammonia uptake by plants from the soil solution and $Q_{[NO_3]}$ is the specific (for unit area) nitrate loss in the hydrologic response ($[M][L^{-2}][T^{-1}]$). Furthermore, MIN is the net mineralization of organic nitrogen into ammonia, $VOLA$ is the rate of NH_4 converted into volatile gases and NIT and $DENIT$ are the nitrification and the denitrification rates, respectively (for a complete description of the biogeochemical model, see Appendix A).

[8] The spatial and temporal distribution of the fertilization rates $F = F_{[NO_3]} + F_{[NH_4]}$ embeds the heterogeneous distribution of the soil types and of the ensuing agricultural practices. We identify four different crop types in the test catchment, namely: maize, wheat, sugar beat and soybean. The average annual nitrogen rates for the above crops are reported in Table 1. Note that the largest annual N load is usually released in maize crops, while the fertilizations applied to the soybean are usually poor of nitrogen. Most of the agricultural fertilizers are chiefly composed by urea and calcium nitrates, with a ratio of 2:1 (two parts of urea per part of nitrate). We assume that maize and sugar beat crops receive their whole annual nitrogen load during the spring (from March to May). Wheat crops are supposed to receive half of their average nitrogen annual load as spring fertilizations and the remaining part as autumn fertilizations (October–November). The average annual load within each subbasin, say $\langle F \rangle$, is thus estimated by averaging the annual load of the different crop types, weighted by their pertinent areal coverage. Accordingly, the average autumnal nitrogen load, $\langle F_a \rangle$, is estimated by weighting the average autumn wheat load with the relative extension of the wheat crops, while the average spring load, $\langle F_s \rangle$, is computed as $\langle F_s \rangle = \langle F \rangle - \langle F_a \rangle$. The random character of the fertilization process is taken into account by a suitable randomization of the fertilization days and loads. The actual nitrogen load released during any simulated year, in fact, is randomly fluctuating around the mean $\langle F \rangle$ following a gaussian distribution with a variation coefficient $CV = 0.1$, while the fertilization days, t_i, are randomly sampled during the spring (March, April, May) and the autumn (October, November) months. Note that the choice of the variation coefficient of the nitrogen load distribution is arbitrary. Finally, the total number of fertilizations per year, say N, is fixed so as the number of spring (N_s) and autumn (N_a) fertilizations can be obtained as $N_s = 3N/5$ and $N_a = 2N/5$, therefore assuming a constant number of fertilization per month during the spring and the autumn. If we neglect the time interval needed for the urea dissolution and for its hydrolisis, the terms $F_{[NO_3]}$ and $F_{[NH_4]}$ in equations (1) and (2) may be easily expressed as:

$$F_{[NO_3]} = \sum_i \varphi_i^{[NO_3]}\, \delta(t - t_i) \quad (3)$$

$$F_{[NH_4]} = \sum_i \varphi_i^{[NH_4]}\, \delta(t - t_i) \quad (4)$$

where $\varphi_i^{[NO_3]}/\varphi_i^{[NH_4]} = 1/2$ and $\delta(\cdot)$ is the Dirac-δ operator. The overall nitrogen load introduced through the i-th fertilization, $\varphi_i = \varphi_i^{[NO_3]} + \varphi_i^{[NH_4]}$, is randomly assigned under the constrain dictated by the conservation of the ensemble average of the spring and autumn nitrogen loads.

[9] The term $Q_{[NO_3]}$ in equation (1), which represents the rate of nitrates leached from the soil solution through the hydrologic response, will be discussed in detail in the next section.

3. Nitrate Leaching

[10] During rainfall events, part of the nitrates stored in immobile soil moisture may be transferred to the mobile water carrier, determining a net leaching of NO_3 in the water runoff. Nitrate circulation in river basins is therefore strongly affected by the space and time variability of rainfall forcings and by nitrate availability in soils. It is well known (and shown elsewhere for the case at hand [*Rinaldo et al.*, 2006b]) that nitrate concentrations in runoff show a pronounced time variability, and relatively large lags of the solute response with respect to the peak of the hydrologic response. This lag has been assumed to stem from the properties of the mass transfer processes from immobile to mobile phases, which is clearly a non-equilibrium process with characteristic time larger than the lead time of water runoff [e.g., *Rinaldo et al.*, 2005, 2006a].

Table 2. Spatially Averaged Physical and Chemical Soil Parameters in the Dese River Basin

Parameter	Symbol	Units	Value	Source
hygroscopic point	s_h	-	0.13	*Rinaldo et al.* [2006b]
wilting point	s_w	-	0.23	*Rinaldo et al.* [2006b]
stomata closure limit	s^*	-	0.39	*Rinaldo et al.* [2006b]
field capacity	s_{FC}	-	0.43	*Rinaldo et al.* [2006b]
porosity	n	-	0.45	*Rinaldo et al.* [2006b]
active soil depth	Z_r	m	0.3	*Rinaldo et al.* [2006b]
soil matric potential exponent	β	-	10.5	*Rinaldo et al.* [2006b]
saturated hydraulic conductivity	K_s	mms^{-1}	0.0025	*Rinaldo et al.* [2006b]
pH	*pH*	-	8.5	*Giandon et al.* [2001]

[11] If nitrate transport in the hydrologic response is modelled by mass response functions (MRF) [*Rinaldo and Marani*, 1987; *Rinaldo et al.*, 1989], one assumes that mass exchange processes occurring within any geomorphic unit (e.g., source areas, channels) are controlled by the travel time distribution of runoff, which also defines the structure of contact times between mobile and immobile phases available for mass transfer processes [*Rinaldo and Marani*, 1987; *Botter et al.*, 2005; *Rinaldo et al.*, 1989, 2005, 2006a]. The nitrate flux $Q_{[NO_3]}(t)$ produced by an arbitrary sequence of net rainfall depths, J ([L]), at the outlet of a single unit in which the catchment is partitioned, may be derived on the basis of its travel time distribution $f(t)$ as:

$$Q_{[NO_3]}(t) = \int_0^t J(t')\, C(t-t', t') f(t-t')\, dt' \tag{5}$$

where C indicates the nitrate concentration in mobile phase; t' is the time at which any single rainfall pulse enters the control volume; t is the current time; and $\tau = t - t'$ is the actual travel time (i.e., the contact time between the immobile phase and the water particles injected as rainfall at time t'). The closure of the problem is ensured by the reaction kinetics governing the time evolution of the nitrate concentration of the water carrier [*Rinaldo et al.*, 2005, 2006a]:

$$\frac{\partial C(\tau, t')}{\partial \tau} = \alpha \left[\frac{[NO_3](\tau + t')}{k_1} - C(\tau, t') \right] \tag{6}$$

where α is the mass transfer rate between the mobile and the immobile phases. The initial conditions for the reaction equation (6) is specified by the nitrate concentration in the soil-water system at the beginning of the rainfall event, which shall be provided by the biogeochemical model described in the previous section.

[12] MRFs require the coupling with a suitable hydrologic model able to provide estimates of the following basic ingredients: i) the amount of net rainfall pertaining to each subbasin, $J(t)$, which is derived from the spatial distribution of rainfall and of relevant hydrologic properties of soil, land-use and vegetation; ii) the description of the travel time distributions $f(t)$ within all the geomorphic units (whether channels or overland areas) and the ensuing geomorphologic unit hydrograph, which embeds the hydrologic response of a complex catchment (where the spatial organization of network connectivity is crucial to large-scale transport processes [see, e.g., *Rinaldo et al.*, 2006a; *Tucker et al.*, 2000]).

[13] A continuously updated description of soil saturation dynamics within each subbasin is achieved by the use of the Green-Ampt model for shallow soils [e.g., *Dingman*, 1994]. The Green-Ampt approach is based on a local water mass balance, which takes into explicit account long-term evapotranspiration processes affecting the soil water balance. To this end, we employ the Penman-Monteith equation integrated by the FAO approach [*Rinaldo et al.*, 2006b], which allows a theoretically sound evaluation of evapotranspiration through (relatively) few micro-meteorological, soil and vegetation parameters, whose spatial distribution has been determined via remotely sensed images. The soil physical and chemical parameters (Tables 2 and 3) have been derived by calibration or via field measurements [see also *Rinaldo et al.*, 2006b]. As a result, the temporal evolution of the soil water content, $s(t)$, and of the transpiration rates, $Tr(t)$, altogether with the spatial distribution of the rainfall volumes contributing to runoff, is achieved from climatic and rainfall data. Transport of the effective rainfall within each subbasin, and the ensuing catchment scale processes, are then modelled following the geomorphological theory of the hydrologic response. Accordingly, the catchment is thought of as a nested structure of geomorphic units, where the spatial distribution of the runoff paths defines the characters of the travel time distribution at the outlet of the basin. The units where paths originate (i.e., the subbasins of the catchment) are labeled by an area A_i whose size (e.g., $\sqrt{A_i}$) has been chosen to be smaller than the correlation scale of rainfall events. The overall catchment-scale travel time distribution, $f_T(t)$, is thus obtained by averaging individual paths' residence time distributions - which are in turn expressed by suitable convolutions of the travel time distributions within the channels, $f_{c_i}(t)$, and the hillslopes, $f_{A_i}(t)$. Exactly derived from proper momentum balance equations, the inverse Gaussian distribution has been used for the probability density function of residence times in the channel reaches, $f_{c_i}(t)$. Instead, exponential distributions are used for the residence times in the hillslopes, $f_{A_i}(t)$, to blend all uncertainties in one parameter (i.e., the mean travel time). Flow discharges are then obtained by routing net rainfall impulses, as provided by the water balance model, with the catchment-scale travel time distribution $f_T(t)$. Details on the analytical framework allowing the description of general arrangements of interconnected geomorphic units, and issues on how to combine coupled flow and transport phenomena in complex

Table 3. Chemical and Biological Parameters of the Nitrogen Model in the Dese River Basin

Parameter	Equation	Units	Value	Source
k_1	(A1)	-	0.18	*Rinaldo et al.* [2006b]
k_2	(A2)	-	5	*Buss et al.* [2004]
μ_D	(A3)	d^{-1}	$1.5 \cdot 10^{-3}$	*Lin et al.* [2000]
β	(A3)	-	1.1	*Lin et al.* [2000]
μ_N	(A4)	d^{-1}	0.5	*Schjønning et al.* [2003]
μ_v	(A5)	d^{-1}	$1.7 \cdot 10^{-1}$	*Martin and Reddy* [1997]; *Rao et al.* [1984]
$(C/N)_b$	(A6)	-	8	*Birkinshaw and Ewen* [2000b]
$(C/N)_h$	(A6)	-	12	*Violante* [1996]
$(C/N)_l$	(A6)	-	30	*Violante* [1996]
k_h	(A6)	$m^3\ d^{-1}\ gN^{-1}$	$2.5 \cdot 10^{-6}$	*Porporato et al.* [2003]
k_l	(A6)	$m^3\ d^{-1}\ gC^{-1}$	$6.5 \cdot 10^{-6}$	*Porporato et al.* [2003]
r_r	(A6)	-	0.7	*Weil et al.* [1988]
r_h	(A6)	-	0.25	*Porporato et al.* [2003]; *Brady and Weil* [1996]
$[C]_b$	(A6)	$gC\ m^{-3}$	8	*Giandon et al.* [2001]
$[C]_h$	(A6)	$gC\ m^{-3}$	9000	*Giandon et al.* [2001]
$[C]_l$	(A6)	$gC\ m^{-3}$	1500	*Giandon et al.* [2001]

networks are reported elsewhere [e.g., *Rinaldo et al.*, 2006a, 2006b].

[14] The hydrologic and nitrate transport model described in this section has allowed a robust estimate of event-based hydrologic and chemical parameters observed in the same catchment considered in this study. Therefore we refer to *Rinaldo et al.* [2006a, 2006b] for the calibration and the discussion of mass transfer rates, hydraulic conductivities and other physical parameters defining the travel time distributions in this basin. Suffice here to mention the good results obtained after the validation of the catchment model of nitrate circulation at the closure of the Dese-Zero test catchment (section *B* in Figure 1, see also section 1). A sample of the comparative analysis of measured and computed results for (a) flux concentrations of nitrates and (b) flowrates is shown in Figures 2a and 2b where the capabilities of the model to reproduce complex hydrologic events are illustrated. Note that the field observations in section B were gathered in a tidal reach (where the flowrates fluctuate widely, see Figure 2b). In contrast the nitrate flux concentration (Figure 2a) does not fluctuate, a feature required of realistic transport models.

4. Climate and Rainfall Models

[15] The stochastic nature of equations (1) and (2), as recently outlined by, e.g., *D'Odorico et al.* [2003] and *Porporato et al.* [2003], stems from the random character of the climatic and hydrologic variables (e.g., temperature, soil water content), which control the mass fluxes across the top soil layer (i.e., the right-hand side terms of the equations (1) and (2)). The uncertainties in predicting the ongoing climate and rainfall regimes are therefore reflected by the uncertain estimates of the nitrogen availability in the soil and of nitrate releases through the hydrologic response. Thus, a probabilistic framework is required to describe the intertwined processes responsible for determining the biogeochemical catchment response (e.g., mass fluxes and storage terms), including the synthetic generation of climate and rainfall series and the simulation of the (hydrologic and biogeochemical) catchment response to prescribed climate and rainfall conditions.

[16] The stochastic generation of rainfall series in the Dese catchment is obtained through the application of a (seasonally-variable) cluster-based rainfall model of the Bartlett-Lewis type [see, e.g., *Rodriguez-Iturbe et al.*, 1987, 1988]. Owing to the limited extent of the Dese catchment with respect to the characteristic size of rainfall events [*Rinaldo et al.*, 2005, 2006b], we employ a zero-dimensional model, therefore assuming spatially uniform rainfall rates throughout the basin. It should be noted, however, that the resulting net rainfall shows a pronounced spatial variability because of the heterogeneity of the hydraulic soil properties. According to the Bartlett-Lewis approach, rainfall is thought of as a series of storms whose inter-arrival times are exponentially distributed with mean λ (see Table 4). Each storm origin is followed by a random number of rectangular cells (whose duration and intensities are exponentially distributed with means $1/\eta$ and μ, respectively, see Table 4), such that the total intensity at any time is the sum of the intensities of all cells active at that time. Moreover, both the inter-arrival times between two subse-

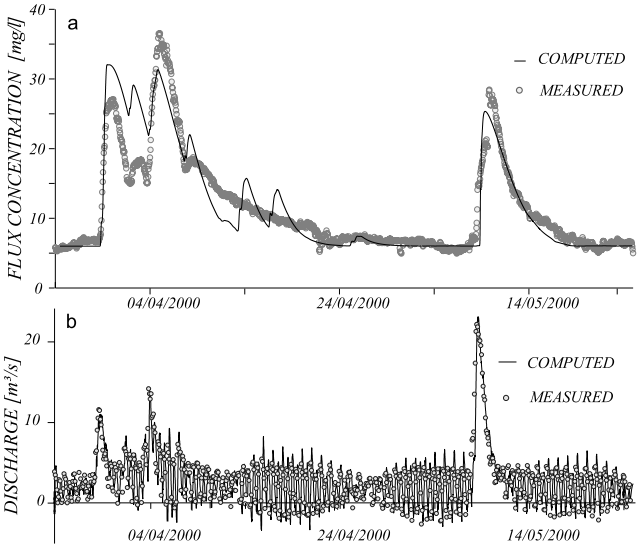

Figure 2. Validation of the nitrate (a) and hydrologic (b) transport models [after *Rinaldo et al.*, 2006b].

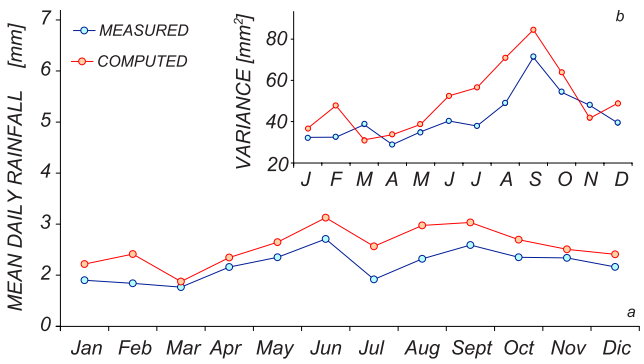

Figure 3. Mean (a) and variance (b) of the modelled daily rainfall (values obtained from a 100-years run) compared with a set of 30-years measured data recorded at the meteorological station of Mestre.

quent cells and the times at which the cell generation stops are exponentially distributed with parameters β and γ, respectively. Finally, the parameter controlling the distribution of the cell duration, η, is assumed to be Gamma-distributed with parameters ν and α [*Rodriguez-Iturbe et al.*, 1988]. The calibration of the model was based on observed average daily rainfall, variance of the 24 and 48-hours cumulative rainfall, 24 and 48-hours dry fractions and on lag-1 (hr) temporal autocorrelation. In order to avoid non-stationarity issues and to reproduce the natural temporal variability, the calibration has been performed on a monthly basis. Figure 3 shows the mean and the variance of the modelled daily rainfall (obtained from a 100-year run) compared to the pertinent statistics derived from a set of 30 years of measured data (recorded at a nearby meteorological station). We note that the accuracy of the model in reproducing the statistical properties of the observed rainfall is somewhat rough, as both the mean and the variance of the daily rainfall are systematically overestimated. We deem, however, that the observed bias of the rainfall model does not significantly affect the results shown in this paper. The complete set of calibrated parameters is reported in Table 4.

[17] The synthetic generation of climatic series has been achieved by the use of a stochastic multivariate ($AR(1)$) daily model which preserves the observed correlations between climatic variables [e.g., *Matalas*, 1967; *Bras and Rodriguez-Iturbe*, 1993]. In order to reduce the complexity of the model, we focus on five climatic variables, which are assumed to control the hydrologic and biogeochemical response of the system: the maximum and minimum daily temperatures (T_{min} and T_{max}), the maximum and minimum relative humidities (Rh_{min} and Rh_{max}) and the wind speed (W_s). In order to preserve the existing auto- and cross-correlations, the current value of each climatic variable is obtained as the sum of a gaussian noise and a suitable linear combination of the values assumed the previous day by all the climatic variables involved. The fluctuations in the correlation between climatic variables and rainfall depths are accounted for by dividing the observed daily climatic variables into three groups [*Srikanthan*, 1985]: wet days followed by wet days; dry days followed by dry days; transition (wet/dry) days. Accordingly, three specific correlation matrices are derived in order to represent the different behavior of each group, w e alternation of the parameters employed for the synthetic generation of the climate data is commanded by the temporal evolution of the modelled daily rainfall. The seasonal variability of daily climatic data is taken into account by considering each month separately. A sample realization of the climate series generated by the $AR(1)$ model is reported in Figure 4, where a comparison is shown with observed climatic properties. From Figures 4a and 4b one notices the good match between the monthly averages of (maximum and minimum) humidity and temperature. Figures 4c and 4d also show a comparison between the observed, (c), and simulated, (d), cross-correlations between different couples of climatic variables. The lower graphs of Figure 4 suggest that the temporal evolution of the cross correlations is reproduced reasonably well by the model.

5. Results and Discussion

[18] The hydro-chemical response of the Dese catchment to the observed climate and rainfall regimes has been reproduced via a Montecarlo application of the stochastic models described above. First, a rainfall series of 100 years has been generated at hourly time steps through the Bartlett-Lewis model. Then, depending on the state (dry/wet) of the current and the previous days, a synthetic series of daily climatic variables has been generated by the AR(1) multivariate climate model (section 4). Next, the hydrologic model is run to estimate: the spatial and temporal distribution of the net rainfall, the soil water content $s(t)$ and the relevant hydrologic fluxes (e.g., transpiration rates, infiltration rates, discharge at the closure of the catchment). Finally, the temporal evolution of the nitrogen concentration in the whole soil-water system is obtained by applying the biogeochemical model described in section 2 (equations (1) and (2)), where the leaching component is computed by the application of equation (5) suitably convoluted to portray the complexity of the geomorphic structure of the catchment [see *Rinaldo et al.*, 2006b]. Figure 5 summarizes some results from the Montecarlo simulation for a sample period of three years. The rainfall intensities are reported in the upper graph (Figure 5a). Daily and seasonal fluctuations clearly appear. Figure 5b plots the maximum daily temperature in time, which also shows significant fluctuations on daily to monthly time scales. As a result, the temporal evolution of the spatially averaged soil water content

Table 4. Calibration Parameters of the Bartlett-Lewis Rainfall Model

Month	λ, h^{-1}	ν, h	α	β/η	γ/η	μ, mm/h
Jan	$7.4 \cdot 10^{-3}$	5.28	11.0	7.72	$9.17 \cdot 10^{-2}$	0.237
Feb	$8.4 \cdot 10^{-3}$	0.63	4.32	9.79	$4.62 \cdot 10^{-2}$	0.235
Mar	$9.3 \cdot 10^{-3}$	$4.25 \cdot 10^{-2}$	2.98	3.00	$1.08 \cdot 10^{-2}$	1.321
Apr	$1.1 \cdot 10^{-2}$	6.83	8.66	6.42	0.147	0.205
May	$1.3 \cdot 10^{-2}$	3.41	6.32	1.98	0.186	0.988
Jun	$1.4 \cdot 10^{-2}$	1.83	8.67	3.03	$7.59 \cdot 10^{-2}$	0.785
Jul	$9.6 \cdot 10^{-3}$	1.13	5.51	4.81	0.272	1.532
Aug	$9.1 \cdot 10^{-3}$	5.62	8.21	3.44	0.228	0.849
Sep	$9.4 \cdot 10^{-3}$	0.14	4.97	11.1	$2.58 \cdot 10^{-2}$	0.739
Oct	$8.6 \cdot 10^{-3}$	0.20	4.01	9.14	$2.11 \cdot 10^{-2}$	0.394
Nov	$9.4 \cdot 10^{-3}$	0.22	4.16	3.97	$1.86 \cdot 10^{-2}$	0.680
Dec	$8.9 \cdot 10^{-3}$	0.51	5.68	6.48	$2.71 \cdot 10^{-2}$	0.386

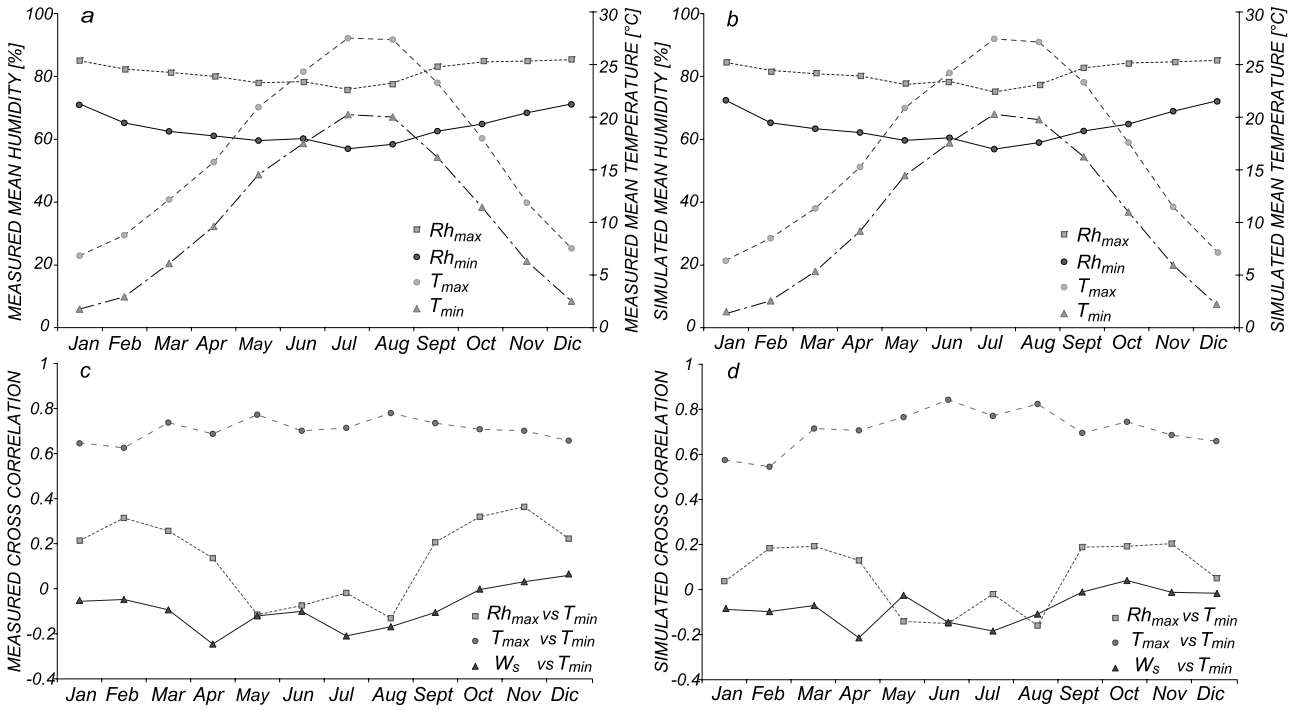

Figure 4. Comparison between monthly average values of observed, (a), and simulated, (b), daily climatic variables: maximum humidity (squares), minimum humidity (black circles), maximum temperature (light gray circles) and minimum temperature (triangles). The lower graphs also shows a comparison between the observed, (c), and simulated, (d), cross correlations between climatic variables: maximum humidity and minimum temperature (squares); maximum temperature and minimum temperature (solid circles); wind speed and minimum temperature (triangles).

(Figure 5c) shows a pronounced temporal variability which reflects the proper climatic and hydrologic processes. Owing to the soil properties and the hydrology of the area [*Giandon et al.*, 2001] irrigation is deemed negligible. The ensuing water discharge at the outlet of the Dese catchment is shown in Figure 5d. Flowrates depend on the soil saturation dynamics and their fluctuations are dominated by high frequency modes characteristic of the short-term hydrologic response, mostly triggered by the occurrence of soil saturation. On the basis of observational evidences [*Rinaldo et al.*, 2006b], we assumed a constant base flow of about 1 m^3/s, which embeds the effect of different sources (i.e., external waters chiefly due to the channel heads fed by shallow water tables and scattered wastewater inputs) not explicitly included in the hydrologic model. Figure 5e shows the temporal evolution of the nitrogen input introduced as fertilizer, expressed as kg of total nitrogen per unit area of agricultural surface. For this application we assumed an overall nitrogen supply of 140 [kg N ha^{-1} $year^{-1}$]. The above nitrogen load has been derived averaging the lower limits of the ranges provided in Table 1 and will thus be employed to assess the minimum impact of agriculture on the biogeochemical processes within the Dese catchment. The effects of the fertilizer on nitrates leaching is illustrated by Figure 5f, where the temporal evolution of nitrate flux in the hydrologic response is shown. Following experimental evidence, we assume a constant nitrate concentration in the base flow (~4 mg/l), which incorporates the effect of different types of point sources (e.g., urban or i ial).

[19] The chemical output signal closely reflects the temporal variability of the hydrologic flow and of the amount instantaneously stored in immobile phases. One may notice that intense nitrate fluxes correlate well with high nitrate concentrations in the soil moisture (in this case, in particular, during the spring of the second and of the third year, see Figure 5g). This suggests that the joint probability of heavy rainfall and high nitrate availability in soil plays a crucial role in triggering the largest NO_3 leaching episodes. Thus, extreme rainfall events cannot be considered as the sole cause of enhanced solute leaching, unless their timing is considered.

[20] Another interesting feature emerges from the analysis of the temporal evolution of nitrate and ammonia soil-water content, shown in Figure 5g. In fact, the dynamics of nitrate concentration in the soil moisture are mostly driven by the fertilizations applied during the growing seasons, whereas high-frequency fluctuations related to small-scale variabilities in soil moisture are small compared to anthropogenic disturbances which maintain the soil-water system far from its biogeochemical equilibrium. This has been shown not to be the case in some water-controlled ecosystems [*Porporato et al.*, 2003], where the dynamics of the nitrates exhibit both small-scale and seasonal fluctuations, the former chiefly controlled by soil-moisture and the latter determined by long term biogeochemical cycles.

[21] Following the Montecarlo approach addressed above, the probabilistic structure of the hydrologic and solute response of the Dese catchment can be reconstructed by analyzing the temporal fluctuations of the hydro-chem-

ical output signals during long-term continuous simulations. Figure 6 shows the probability density functions of (relative) soil moisture computed from a 100-years run of the model for different seasonal regimes, i.e., those derived from the climatic parameters of March to May (circle) and from June to August (triangles). The skewness of the distribution changes from negative to positive as the average rainfall intensity increases. It is worthwhile to mention that this effect is shown in the exact probabilistic model of *Rodriguez-Iturbe et al.* [1999] for a homogeneous soil. Indeed, for the sake of comparison, Figure 6 also shows (continuous lines) the steady-state soil moisture probability density function (pdf) derived by *Rodriguez-Iturbe et al.* [1999] where we have performed a suitable calibration only of the maximum evaporation and evapotranspiration rates. The good match between the soil moisture pdf derived from the Montecarlo simulation and the results of the model proposed by *Rodriguez-Iturbe et al.* [1999] is somewhat broader than the successful comparison against field data already evidenced for homogeneous soils [*Salvucci*, 2001]. Here, in fact, we are comparing soil moisture at catchment scales where soils and land uses are rather heterogeneous, and their intertwined effect on runoff production fully considered. The fact that indeed there exists an effective state averaging highly heterogeneous properties opens new avenues for application of the exact model of *Rodriguez-Iturbe et al.* [1999] and proves the flexibility of the Montecarlo approach described here to tackle manned catchments, where spatially-averaged soil moisture pdf should be described by large-scale rainfall and vegetation macroscopic (or effective) parameters.

[22] Differently from most current models, where the nitrate leaching is empirically treated as proportional to runoff, the nitrate transport model adopted here allows for much variable ratios, r, between the nitrate concentration in the runoff and the actual nitrate content of the soil moisture. The modelled probability density function of r in the Dese catchment (computed from the 100-year hourly simulation) is reported in Figure 7, which emphasizes the occurrence of large fluctuations. This complies with convincing observational evidences [*Rinaldo et al.*, 2006b].

[23] The effect of the anthropogenic disturbance on nitrogen availability in soil moisture may be further investigated by analyzing the (modelled) monthly $[NO_3]$ probability distributions. Figure 8 shows how agricultural inputs through fertilizations (Figures 8a and 8c) may lead to bimodal $[NO_3]$ pdfs, where large $[NO_3]$ values are characterized by high occurrence probabilities. In the growing

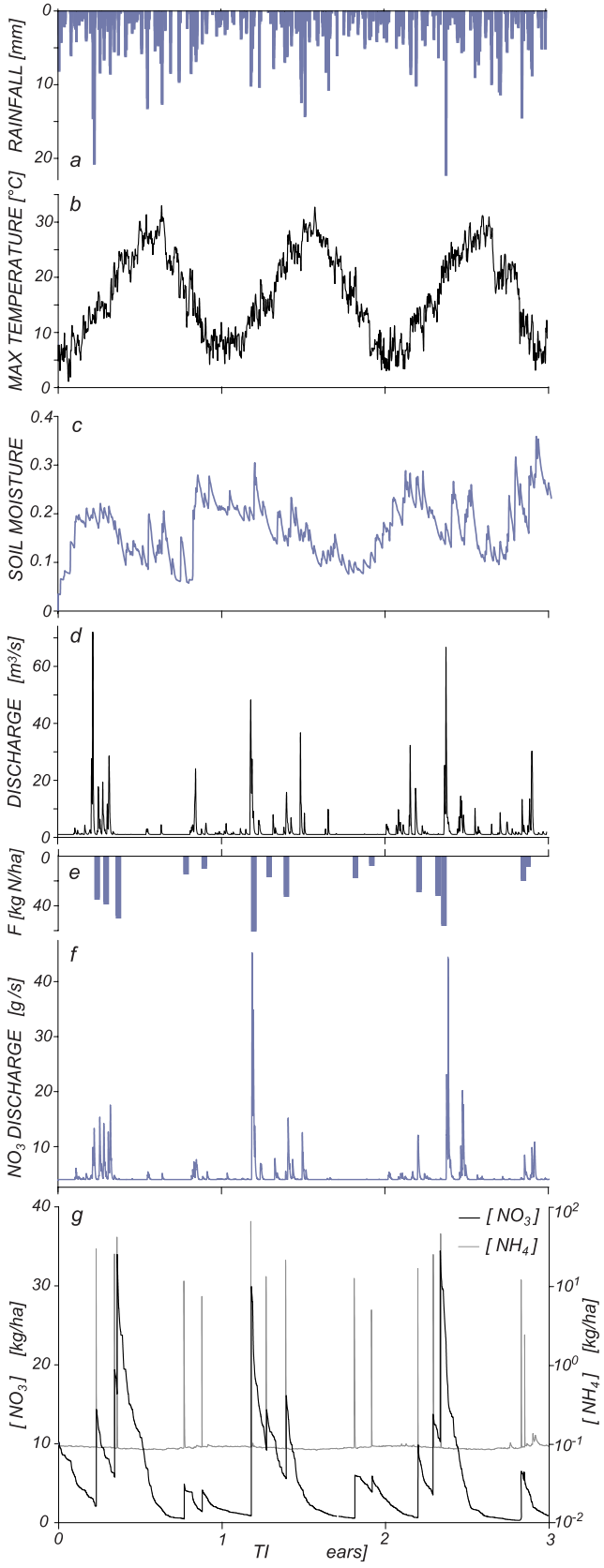

Figure 5. Output from the Montecarlo simulation of the rainfall, climate, hydro and biogeochemical models described in sections 2, 3, and 4. Relevant pluviometric, climatic, hydrologic and chemical properties are plotted during a sample period of three years: (a) rainfall heights; (b) maximum daily temperature $T_{max}(t)$; (c) mean daily soil water content in the top soil layers averaged over the whole basin, $n \cdot s(t)$. Note that the averaging procedures becloud saturation events that, when they occur, typically last only a few hours and do not necessarily involve simultaneously all sites; (d) discharge at the closure of the Dese basin (section A in Figure 1); (e) temporal variability of the nitrogen input introduced as fertilizers, $F(t)$; (f) nitrate leaching through the hydrologic response at the control section, $Q_{[NO_3]}(t)$; (g) temporal evolution of the nitrate (dark line) and ammonia (grey line) concentration in the top soil layer.

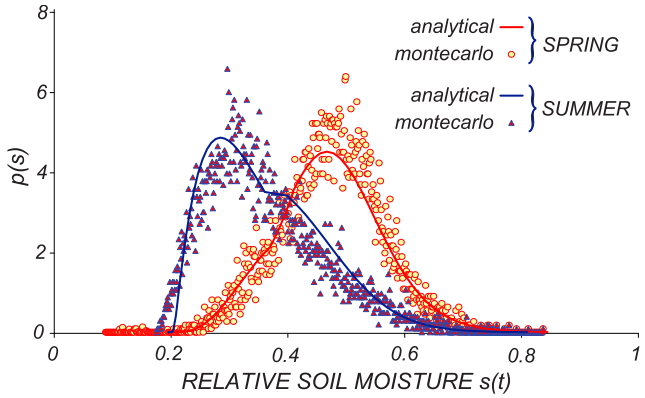

Figure 6. Statistical properties of the hydrologic and chemical output signal derived from a 100 years Montecarlo application of the rainfall, climate, hydro and biogeochemical models: the modelled probability density functions of the relative soil moisture during the springtime and in Summer are labelled with dots and triangles, respectively. For the sake of comparison, the steady-state pdfs proposed by *Rodriguez-Iturbe et al.* [1999] and *Laio et al.* [2001] are reported as continuous lines. The uncalibrated spatially averaged soil parameters are reported in Table 2. The rainfall parameters (the average interarrival time between storms, λ^{-1}, and the average daily rainfall depth, α) have been derived on the basis of the synthetic rainfall series: in Springtime $\lambda = 0.3$ [d^{-1}] and $\alpha = 8.0$ [mm], whereas in Summer $\lambda = 0.28$ [d^{-1}] and $\alpha = 8.3$ [mm]. The calibrated maximum evaporation, E_w, is 6.3 10^{-3} [cm d^{-1}] in both cases, while the maximum evapotranspiration, E_{max}, is 0.13 [cm d^{-1}] for the spring and 0.25 [cm d^{-1}] in summer. See *Laio et al.* [2001] for further details on the analytical expression of $s(t)$.

season, in fact, and particularly during the spring (when most of the fertilizer is released onto the soils), the natural [NO_3] pdf (Figure 8b) is significantly skewed to the left. The soil-water system seems to retain a long memory of the disturbances in the nitrate pool, where a new biogeochemical equilibrium may be reached only several weeks after the disturbance (see also Figure 5g). As a result, the overall

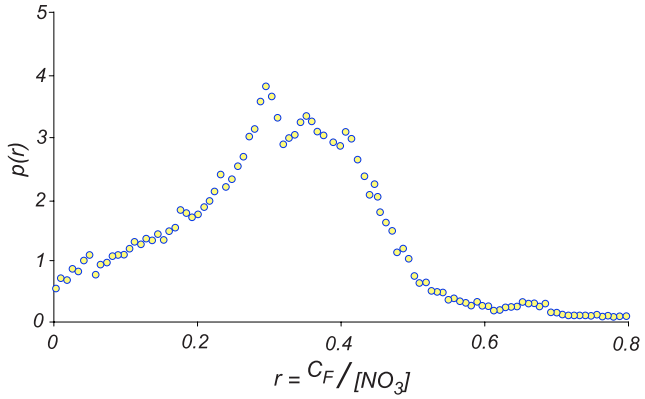

Figure 7. Probability density function of the ratio between the flux concentration at the outlet of the Dese catchment, C_F, and the spatially averaged nitrate concentration in the soil-water system, [NO_3]

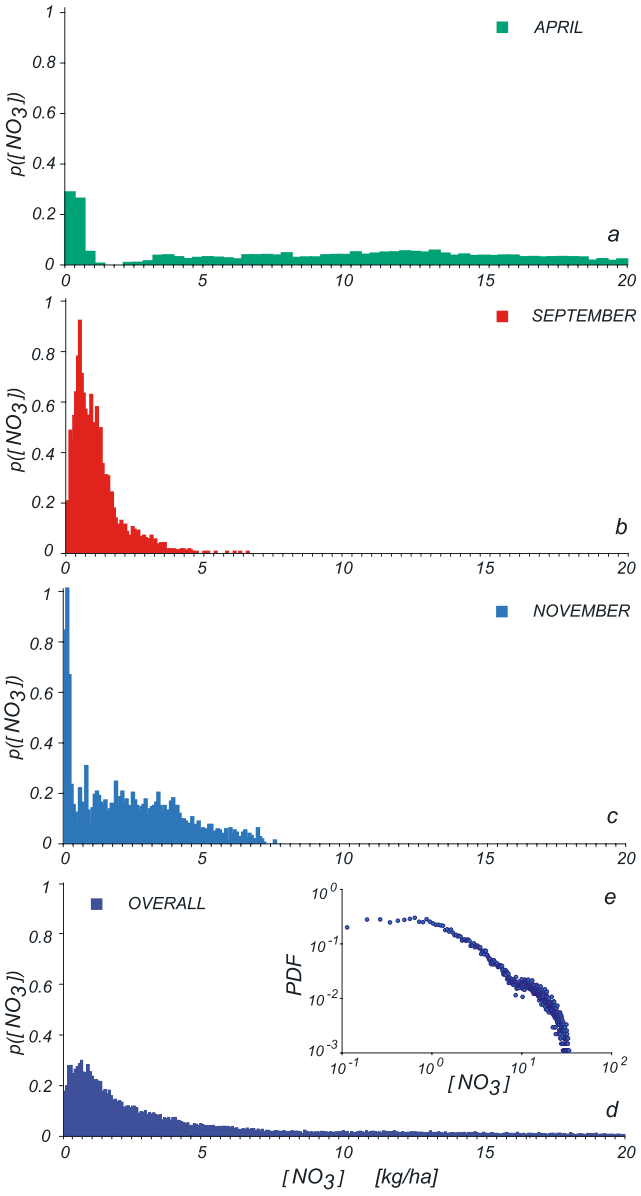

Figure 8. Probability density function of the nitrate concentration in the soil-water system for different time periods: April (a), September (b) and November (c); (d) overall probability density function of the nitrate concentration in the soil-water system during a 100-years Montecarlo simulation. The inset (e) reports a log-log plot of the overall [NO_3] pdf which suggests large occurrence probabilities for high NO_3 concentrations.

yearly pdf of nitrate concentration in the soil moisture exhibits a relatively long tail (Figures 8d and 8e), with a sharp cut-off around the maximum NO_3 load introduced as fertilizers. Were this confirmed, it would have implications on increased risks of enhanced NO_3 leaching. The increased probability of nitrate leaching during spring rainfall events is also suggested by Figure 9, showing the temporal evolution of the average daily nitrates load and runoff (a), as well as the corresponding normalized variances (b). The average daily runoff shows a weak temporal variability with a maximum during the autumn, which nearly reflects the increase in rainfall volumes. Conversely, the average daily

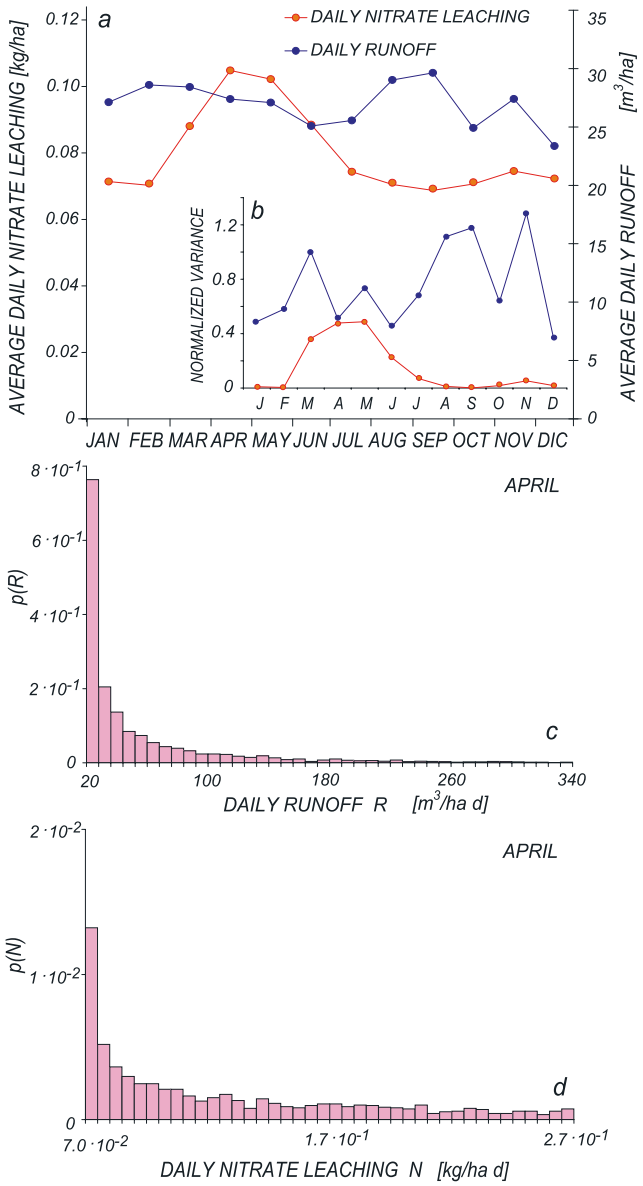

Figure 9. (a) Monthly averages of daily nitrate loads, $\langle N \rangle$, and runoff, $\langle R \rangle$. The corresponding monthly normalized variances ($Var(N)/\langle N \rangle^2$ and $Var(R)/\langle R \rangle^2$) are reported in the inset (b). April pdfs of the daily runoff (c) and of the daily nitrates leaching (d). Note that the pdfs reported in c and d neglect the atom of probability corresponding to the absence of hydrologic flow, in this case 0.19.

nitrate leaching and the corresponding normalized variance show a pronounced increase during the spring owing to the high nitrogen availability. Figures 9c and 9d suggest differences in structure of the April pdf of the daily runoff (which exhibits a nearly exponential behavior) and the longer-tailed distribution of daily nitrate fluxes. The complex mechanisms through which the inflowing rainfall volumes are eventually transformed into water discharges and nitrate loads are also highlighted by the pdf of the modelled daily rainfall, of the daily discharge and of the daily nitrate leaching (Figure 10). The soil-saturation dynamics change the structure of the outflow scharges with respect to the inflowing rainfall volumes (Figures 10a and 10b). However, the above damping effect tends to decrease as the relative intensity of the inflowing rainfall increases, suggesting that high rainfall rates produce intense runoff mostly driven by rapid (i.e., surface) processes. The basin-scale nitrate response, instead, shows a somewhat different behavior as suggested by some resemblance to a power-law distribution (with exponent ~1.6) characterizing daily nitrates leaching (Figure 10c). It is premature to conclude that the model produces scaling load distributions, as the range of scales covered is not wide enough. It remains significant, however, the tendency shown by the probability distributions. The complex hydro-biogeochemical transformations within the soil-water system produce nitrate output fluxes much smaller than the corresponding inputs (a few decades of kg ha^{-1} d^{-1} during the fertilization days). Conversely, the probabilistic structure of the chemical output signal (i.e., the pdf of nitrate output loads) ensures relatively high occur-

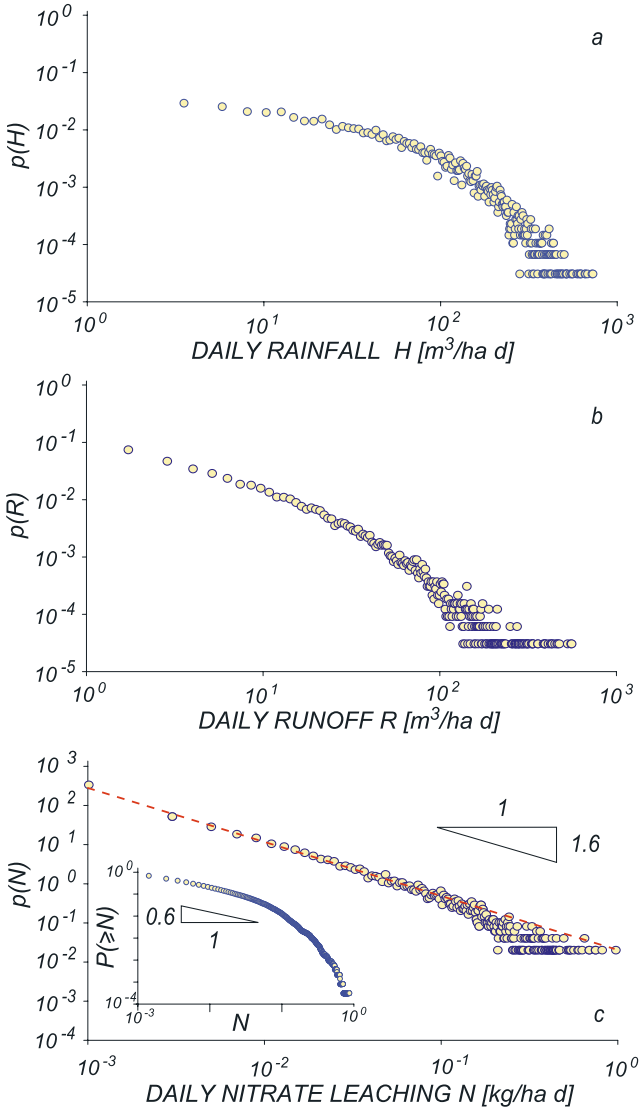

Figure 10. Simulated probability density functions of daily rainfall (a), runoff (b) and nitrate leaching (c). The inset reports the cumulative probability for the daily nitrate leaching.

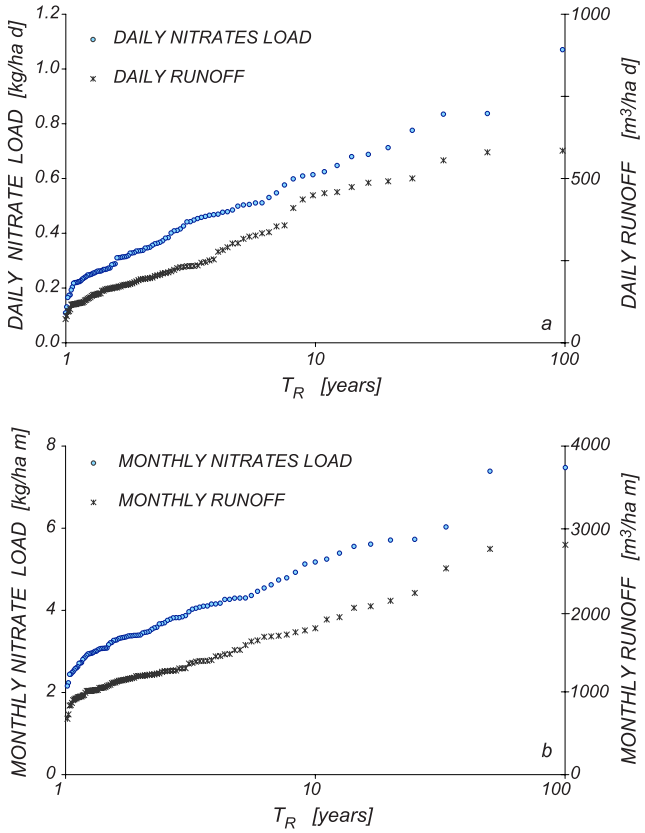

Figure 11. Statistical properties of the modelled hydrologic and nitrate responses in the Dese catchment: (a) return period of the daily nitrate load (dots) and of the daily runoff (crosses); (b) return period of the monthly nitrate load (dots) and of the monthly runoff (crosses). A constant base-flow is included in both data sets.

rence probabilities for extreme events, due to the power-low type behavior of the leaching pdf.

[24] The Montecarlo approach described here allows for a robust estimate of the statistics of nitrate releases and runoff. In particular, from the annual maxima of the nitrate loads and of the water volumes released to the receiving water body, one may estimate the return period of the corresponding hydro-chemical output fluxes. The intensity-frequency curves for the (daily and monthly) nitrate load and for the (daily and monthly) runoff reported in Figures 11a and 11b show that the extreme nitrate loads exhibit a strong dependence on their relative frequency: the maximum daily nitrate load is, in fact, about 10 times larger than the daily load exceeded on the average every year (Figure 11a), while the daily runoff corresponding to a return interval of 100 years is only 4 to 5 times bigger than the daily runoff volume with a return period of one year. The time variability of the daily hydrologic response, in fact, is chiefly due to the intermittency which characterizes the temporal distribution of rainfall, while important yearly fluctuations in the nitrate response are also related to the fluctuations in the undergoing climatic and biogeochemical processes. It is worth mentioning that extreme nitrate leaching and extreme runoff volumes do not originate from the same rainfall events. The return period of the water volumes released during extreme (daily and mo nitrate leaching, in fact, is rather low (of the order of 2 years), and vice versa. This is due (possibly in general) to the fact that the heaviest rainfall episodes usually occur during the fall season, while the largest availability of nitrates prone to hydrologic leaching can be found in springtime as commanded by the agricultural practice.

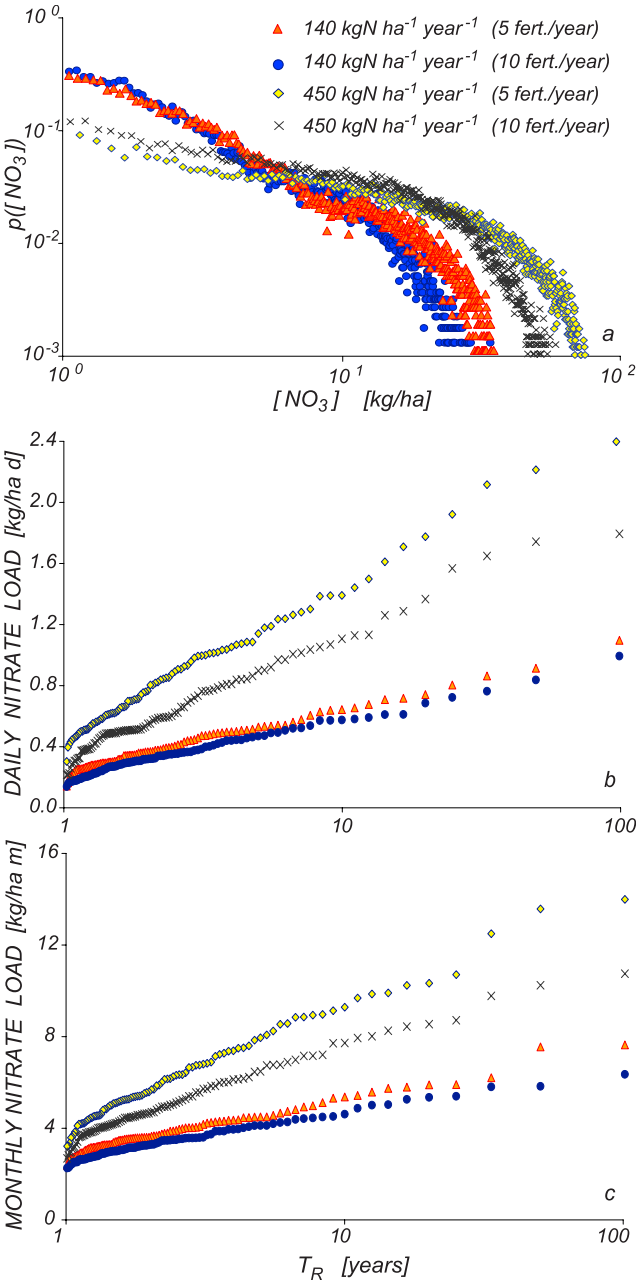

Figure 12. Effect of different fertilization strategies on the $[NO_3]$ pdf in soil (a) and on the return period of the daily (b) and monthly (c) nitrate loads: i) 140 [kg N ha^{-1} year^{-1}] introduced by means of 10 fertilizations per year (dark dots); ii) 140 [kg N ha^{-1} year^{-1}] introduced by means of 5 fertilizations per year (triangles); iii) 450 [kg N ha^{-1} year^{-1}] introduced by means of 5 fertilizations per year (light dots); iv) 450 [kg N ha^{-1} year^{-1}] introduced by means of 10 fertilizations per year (crosses).

[25] The ability of the model to simulate future scenarios and testing the effects of remediation strategies is shown by an illustrative example which analyzes the effects of different fertilization strategies on the chemical response of the Dese catchment (see Figure 12). We test four scenarios, where different nitrogen loads are released by means of a different number of fertilizations per year: i) 140 [kg N ha^{-1} $year^{-1}$] introduced by means of 5 fertilizations per year; ii) 140 [kg N ha^{-1} $year^{-1}$] introduced by means of 10 fertilizations per year; iii) 450 [kg N ha^{-1} $year^{-1}$] introduced by means of 5 fertilizations per year; iv) 450 [kg N ha^{-1} $year^{-1}$] introduced by means of 10 fertilizations per year. Needless to say, the above strategies are not be intended as actual scenarios; they simply represent qualitatively different levels of anthropogenic pressure. Figure 12a shows the $[NO_3]$ pdfs computed for the soil-water system. Interestingly, in all the cases reported here the pdf of soil nitrate content shows some signs of a power-law behavior, suggesting that the biogeochemical system tends to have no preferential states. Long memory of external disturbances could also be assessed by analyzing the covariance functions of time series of nitrates contents, fluxes and concentrations. For a prescribed annual nitrogen load, the increase of the number of yearly fertilizations, N, produces a significant leftward shift of the cut-off, without substantially altering the shape of the pdf. Conversely, the strongest control on the nitrate probability distribution is played by the total annual nitrogen load introduced as fertilizer, which affects the scaling exponent of the pdf - issues of its adaptation to a scaling distribution aside. The intensity-frequency curves for the daily and monthly nitrate loads resulting from the different fertilization plans investigated are reported in Figures 12b and 12c. As expected, the probability of intense nitrate releases decreases both with the partitioning of the total fertilizer load into a larger number of fertilizations and with the use of decreasing values of total anthropogenic loads. The increase in the number of yearly fertilizations produces remarkable effects on the extreme daily nitrate loads only when huge amounts of nitrogen are externally applied. The relative impact of the fertilization fractioning (i.e., the relative distance between the curves referring to the same average annual load, reported in Figures 12b and 12c), decreases, however, as the corresponding return period increases, suggesting that the largest leaching episodes, which require relatively intense rainfall events, usually do not occur in correspondence to the largest NO_3 concentration in soil. Conversely, Figure 12c shows that the effects of increasing N on the extreme monthly nitrates releases are on the average less pronounced with respect to the case of daily NO_3 leaching. The illustrative example discussed above suggests the potential of the stochastic framework developed in this paper for testing different remediation strategies aiming at, e.g., reduced average flux concentrations, daily or seasonal loads.

6. Conclusions

[26] The following conclusions are worth emphasizing:

[27] 1. A new methodology based on Montecarlo simulations has been developed and applied to a relevant case study by coupling stochastic rainfall and climate generators with hydrologic and biog mical models operating at basin scales where control volumes entail different source areas (whether agricultural or urban) and arbitrarily connected channelizations;

[28] 2. Anthropogenic inputs of agricultural origin, routinely applied to the croplands, produce long-lasting consequences on the biogeochemical equilibrium of the ecosystem, leading to probability distributions of nitrate in storage within the soils differing from the hydrologic variables driving runoff. As a result, we predict the probability of enhanced NO_3 leaching and overall load to the receiving water body.

[29] 3. Extreme nitrate leaching episodes in agricultural basins are eminently controlled by the interplay between intermittent rainfall forcings and nitrogen inputs through fertilizations. The small-scale variability of relevant hydrologic variables (e.g., soil moisture) seems of somewhat lesser importance. We have provided estimates of the seasonal probability distributions of all variables of interest (i.e., daily and monthly releases of water and nitrates in the runoff, soil moisture and nitrate content);

[30] 4. The return period of the daily and monthly nitrate loads and runoff volumes has been estimated. Extreme nitrates loads are found to be mostly triggered by ordinary flood events (i.e., events with low return periods). What matters, therefore, is the joint probability of high nitrogen availability in soil and of significant rainfall events;

[31] 5. Different management scenarios have been tested, providing useful indications on the mechanisms controlling the largest nitrate flushing episodes.

Appendix A: Biogeochemical Model

[32] A brief description of the terms appearing in the biogeochemical model provided by equations (1) and (2) is addressed below. Plants assimilate nutrients from soil moisture through complex mechanisms, whose complete description at the basin scale is hardly feasible - and possibly immaterial. Because agricultural soils are usually characterized by relatively high nitrogen concentrations, we adopt a simplified model which neglects active uptake and assumes that nitrogen availability in soil is always larger than the actual plant demand. Under the above circumstances, nitrate (and ammonia) uptake from the soil solution, $PU_{[NO_3]}$ ($PU_{[NH_4]}$), can be computed as the product between the instantaneous transpiration rates $Tr(t)$ $[L^3T^{-1}]$ - suitably derived from the hydrologic model - and the average nitrate (ammonia) concentration in the soil moisture. We shall assume that the instantaneous concentration of nitrates and ammonia in soil moisture are both proportional to the concentration in the soil-water system (see section 3). The uptake terms in equations (1) and (2) may be thus expressed as [*Porporato et al.*, 2003]:

$$PU_{[NO_3]} = Tr(t) \cdot \frac{[NO_3]}{k_1} \tag{A1}$$

$$PU_{[NH_4]} = Tr(t) \cdot \frac{[NH_4]}{k_2} \tag{A2}$$

where k_1 is a coefficient which embeds the nitrates solubility and the temporal variability of the soil water

content [*Rinaldo et al.*, 2006a, 2006b] and k_2 is the partition coefficient for ammonia.

[33] The NO_3^- denitrification is strictly related to the biological activity of heterotrophic bacteria (e.g., *vibrio denitrificans*) capable of exploiting, in anoxic conditions, the nitrates dissolved in soil moisture as oxygen sources. As a consequence of denitrification processes gaseous N is produced, which is released into the atmosphere. The denitrification rate has been computed as a function of the actual water content $s(t)$ and of the average daily temperature $T(t)$ as follows [e.g., *Lin et al.*, 2000]:

$$DENIT = \begin{cases} \dfrac{\mu_D\, s(t)}{s_{FC}} \beta^{\frac{T(t)-25}{10}} \cdot [NO_3] & if\ s(t) \geq s_{FC} \\ 0 & if\ s(t) < s_{FC} \end{cases} \tag{A3}$$

where S_{FC} represents the field capacity (i.e., the maximum water volume detained against the gravity forces for a unit soil volume), β is a coefficient embedding the dependence of the denitrification rate on the daily temperature and μ_D is the denitrification rate at the optimum temperature of 25° for a unit concentration of nitrates. Note that the denitrification process is completely inhibited when the soil moisture falls below field capacity (and the anaerobic microbial respiration is prevented). Denitrification is instead enhanced by rising temperatures and by high soil water contents. In this study, the temporal evolution od the soil moisture $s(t)$ and the average daily temperature $T(t)$ have been suitably derived from the climatic and hydrologic model, as described in sections 3 and 4.

[34] Nitrification of ammonia is chiefly performed by autotrophic bacteria (e.g., *nitrosomonas*, *nitrobacter*) which use the energy derived from the oxidation of inorganic matter. The nitrification of NH_4 has been thus modelled as a function of the soil water content and of the organic content in the biomass $[C]_b$ [e.g., *Porporato et al.*, 2003]:

$$NIT = \begin{cases} \dfrac{s(t)}{s_{FC}} \cdot \mu_N\, [C]_b [NH_4] & if\ s(t) < s_{FC} \\ \dfrac{1-s(t)}{1-s_{FC}} \cdot \mu_N\, [C]_b [NH_4] & if\ s(t) \geq s_{FC} \end{cases} \tag{A4}$$

where μ_N is the maximum nitrification rate for a unit carbon concentration in the microbial biomass and for a unit concentration of NH_4. For low soil water contents nitrification is partially inhibited and the nitrification rate grows linearly with the soil moisture. The optimum condition for nitrification is achieved when $s(t) = s_{FC}$, while for higher values of the soil moisture the nitrification rate linearly decreases with s.

[35] Under basic conditions ($pH \geq 8$) ammonia may be converted into $N - NH_3$, which is, in turn, rapidly transformed into $N - NH_2$, a volatile gas to be lost into the atmosphere. The ammonia volatilization has been thus modelled as a function of the soil pH [*Martin and Reddy*, 1997; *Lin et al.*, 2000]:

$$VOLA = \mu_v 10^{pH-10}\, [NH_4] \tag{A5}$$

where μ_v is suitable empirical coefficient embedding the dependence of the volatilization rates on climatic and environmental factors.

[36] Mineralization is a reversible chemical process through which organic N is converted into ammonia. When the carbon-nitrogen ratio in the microbial biomass, $(C/N)_b$, is lower than the value required by the microbes ($\simeq$20), the bacteria decomposition results in a nitrogen surplus, which is incorporated by the mineral nitrogen pool. Owing to the low organic content of the biomass and to the large availability of nitrogen, the carbon/nitrogen ratios in the microbial biomass in agricultural soils are usually nearly low. Following *Porporato et al.* [2003] and *Birkinshaw and Ewen* [2000b] we assumed $(C/N)_b = 8$. If we neglect the immobilization of mineral nitrogen, the rate of mineralization of organic nitrogen may be thus computed as a function of the soil water content as:

$$MIN = f_m [C]_b \left\{ k_h [C]_h \left[\frac{1}{(C/N)_h} - \frac{1-r_r}{(C/N)_b} \right] + k_l [C]_l \left[\frac{1}{(C/N)_l} - \frac{r_h}{(C/N)_h} - \frac{1-r_h-r_r}{(C/N)_b} \right] \right\} \tag{A6}$$

where r_h and r_r are the iso-humic and the respiration coefficients, respectively, and k_h and k_l represent decomposition parameters. $(C/N)_b$, $(C/N)_l$ and $(C/N)_h$ represent, respectively, the dimensionless carbon/nitrogen ratios in the biomass, in the litter and in the humus pool, while $[C]_b$, $[C]_l$ and $[C]_h$ are the corresponding organic contents, assumed to be constant. Moreover, f_m in equation (A6) is a dimensionless coefficient which accounts for the dependence of the decomposition rate on the soil water content:

$$f_m = \begin{cases} \dfrac{s(t)}{s_{FC}} & if\ s(t) \leq s_{FC} \\ \dfrac{s_{FC}}{s(t)} & if\ s(t) > s_{FC} \end{cases} \tag{A7}$$

[37] The complete set of biogeochemical parameters required by the nitrogen model is shown in Table 3.

[38] **Acknowledgments.** This research is an outgrowth of the EU project AQUATERRA (contract 505428 - GOCE). Financial support was also provided by CORILA (GB).

References

Birkinshaw, S. J., and J. Ewen (2000a), Nitrogen transformation component for SHETRAN catchemnt nitrate transport modelling, *J. Hydrol.*, *230*, 1–17.

Birkinshaw, S. J., and J. Ewen (2000b), Modelling nitrate transport in the Slapton Wood catchment using SHETRAN, *J. Hydrol.*, *230*, 18–33.

Botter, G., E. Bertuzzo, A. Bellin, and A. Rinaldo (2005), On the Lagrangian formulations of reactive solute transport in the hydrologic response, *Water Resour. Res.*, *41*, W04008, doi:10.1029/2004WR003544.

Brady, N. C., and R. R. Weil (1996), *The Nature and Properties of Soils*, 11th ed., Prentice-Hall, Upper Saddle River, N. J.

Bras, R., and I. Rodriguez-Iturbe (1993), *Random Functions and Hydrology*, Dover, Mineola, N. Y.

Buss, S. R., A. W. Herbert, P. Morgan, S. F. Thornton, and J. W. N. Smith (2004), A review of ammonium attenuation in soil and groundwater, *Q. J. Eng. Geol. Hydrogeol.*, *37*(4), 347–359.

Dingman, S. L. M. (1994), *Physical Hydrology*, MacMillan, New York.

D'Odorico, P., A. Porporato, F. Laio, and I. Rodriguez-Iturbe (2003), Soil moisture controls on the nitrogen cycle. II. A case study, *Adv. Water Resour.*, *26*, 59–70.

Giandon, P., F. Ragazzi, I. Vinci, L. Fantinato, A. Garlato, P. Mozzi, and G. P. Bozzo (2001), La carta dei suoli del bacino scolante in Laguna di Venezia, *Bollettino della Società Italiana della Scienza del Suolo*, *50*, 273–280.

Jordan, C., and R. V. Smith (2005), Methods to predict the agricultural contribution to catchment nitrate loads: Designation of nitrate vulnerable zones in Northern Ireland, *J. Hydrol.*, *304*, 316–329.

Kurz, I., C. Coxon, H. Tunney, and D. Ryan (2005), Effects of grassland management practices and environmental conditions on nutrient concentrations in overland flow, *J. Hydrol.*, *304*, 35–50.

Laio, F., A. Porporato, L. Ridolfi, and I. Rodriguez-Iturbe (2001), Plants in water-controlled ecosystems: Active role in hydrologic processes and response to water stress. II. Probabilistic soil moisture dynamics, *Adv. Water Resour.*, *24*, 707–723.

Lin, B., A. Sakoda, R. Shibasaki, N. Goto, and M. Suzuki (2000), Modelling a global biogeochemical nitrogen cycle in terrestrial ecosystems, *Ecol. Model.*, *135*, 89–110.

Manzoni, S., A. Porporato, P. D'Odorico, F. Laio, and I. Rodriguez-Iturbe (2004), Soil nutrient cycles as a nonlinear dynamical system, *Nonlinear Process Geophys.*, *11*, 1–10.

Martin, J. F., and K. R. Reddy (1997), Interaction and spatial distribution of wetland nitrogen processes, *Ecol. Model.*, *105*, 1–21.

Matalas, N. C. (1967), Time series analysis, *Water Resour. Res.*, *3*, 817–829.

Pastor, J., and W. M. Post (1986), Influence of climate, soil moisture, and succession on forest carbon and nitrogen cycles, *Biogeochemistry*, *2*, 3–27.

Porporato, A., P. D'Odorico, F. Laio, and I. Rodriguez-Iturbe (2003), Soil moisture controls on the nitrogen cycle. I. Modeling scheme, *Adv. Water Resour.*, *26*, 45–58.

Rao, P. S. C., R. E. Jessup, and K. R. Reddy (1984), Simulation of nitrogen dynamics in flooded soils, *Soil Sci.*, *138*, 54–62.

Rinaldo, A., and A. Marani (1987), Basin scale model of solute transport, *Water Resour. Res.*, *23*(11), 2107–2118.

Rinaldo, A., A. Marani, and A. Bellin (1989), On mass response functions, *Water Resour. Res.*, *25*(8), 1603–1617.

Rinaldo, A., E. Bertuzzo, and G. Botter (2005), Nonpoint source transport models from empiricism to a coherent theoretical framework, *Ecol. Model.*, *184*, 19–35.

Rinaldo, A., G. Botter, E. Bertuzzo, A. Uccelli, T. Settin, and M. Marani (2006a), Transport at basin scale: 1. Theoretical framework, *Hydrol. Earth Syst. Sci.*, *10*, 19–30.

Rinaldo, A., G. Botter, E. Bertuzzo, A. Uccelli, T. Settin, and M. Marani (2006b), Transport at basin scale: 2. Applications, *Hydrol. Earth Syst. Sci.*, *10*, 31–48.

Rodriguez-Iturbe, I., D. R. Cox, and V. Isham (1987), Some models for rainfall based on stochastic point processes, *Proc. R. Soc. London A*, *410*, 269–288.

Rodriguez-Iturbe, I., D. R. Cox, and V. Isham (1988), A point process model for rainfall: Further developments, *Proc. R. Soc. London A*, *417*, 283–298.

Rodriguez-Iturbe, I., A. Porporato, L. Ridolfi, V. Isham, and D. Cox (1999), Probabilistic modelling of water balance at a point: The role of climate soil and vegetation, *Proc. R. Soc. London A*, *455*, 3789–3805.

Salvucci, G. D. (2001), Estimating the moisture dependence of root zone water loss using conditionally averaged precipitation, *Water Resour. Res.*, *37*(5), 1357–1365.

Schjønning, P., I. K. Thomsen, P. Moldrup, and B. T. Christensen (2003), Linking soil microbial activity to water- and air-phase contents and diffusivities, *Soil Sci. Soc. Am. J.*, *67*, 156–165.

Srikanthan, R. (1985), Stochastic simulation of daily climatic data, paper presented at Fourth International Hydrology Symposium, Fort Collins, Colo.

Tucker, G., F. Catani, A. Rinaldo, and R. L. Bras (2000), Statistical analysis of drainage density from digital terrain data, *Geomorphology*, *36*(3–4), 187–202.

Vanclooster, M., P. Viaene, J. Diels, and K. Christiaens (1995), A deterministic evaluation analysis applied to an integrated soil-crop model, *Ecol. Model.*, *81*, 183–195.

Violante, P. (1996), *Chimica del suolo e nutrizione delle piante*, Edagricole, Bologna.

Weil, R. R., P. W. Benedetto, L. J. Sikora, and V. A. Bandel (1988), Influence of tillage practices on phosphorus distribution and forms in three Ultisols, *Agron. J.*, *80*, 503–509.

Whitehead, P. G., E. J. Wilson, and D. Butterfield (1998), A semi distributed Integrated Nitrogen model for multiple source assessment in catchment (INCA). Part I. Model structure and process equation, *Sci. Total Environ.*, *210/211*, 547–558.

G. Botter, M. Marani, A. Rinaldo, and T. Settin, Dipartimento di Ingegneria Idraulica, Marittima, Ambientale e Geotecnica, Universitá di Padova, via Loredan 20, I-35131 Padova, Italy. (rinaldo@idra.unipd.it)